THE JOURNAL OF CHEMICAL PHYSICS **122**, 034303 (2005)

Competition between adiabatic and nonadiabatic fragmentation pathways in the unimolecular decay of the $ArI_2(B)$ van der Waals complex

Octavio Roncero
Instituto de Matemáticas y Física Fundamental, CSIC, Serrano 123, 28006 Madrid, Spain

Alexei A. Buchachenko[a] and Bruno Lepetit
LCAR-IRSAMC, Université Paul Sabatier et CNRS, UMR5589, F-31062 Toulouse Cedex, France

(Received 14 September 2004; accepted 22 October 2004; published online 30 December 2004)

The competition between vibrational and electronic predissociations of the $ArI_2(B)$ van der Waals complex has been studied using several dynamical computational methods: exact quantum wave-packet propagation, time-dependent golden rule, and quasiclassical trajectory with quantum jumps model. Five electronic states are considered using recent three-dimensional coupled surfaces obtained with a perturbative diatoms-in-molecules method. Final vibrational and electronic populations, predissociation rates, and absorption spectra have been computed for $I_2(B,v=18-24)\leftarrow I_2(X,v=0)$ excitations within the complex. The contribution of vibrational predissociation into the total decay oscillates as a function of vibrational excitation due to intramolecular vibrational relaxation in a sparse-intermediate regime, which induces irregular variations of the total decay rate. Franck–Condon oscillations control the branching ratios of the individual electronic predissociation channels. However, since these oscillations are out of phase as a function of vibrational excitation, they have limited effect on the oscillatory behavior of the total predissociation rate. Comparison between exact quantum and perturbative golden rule calculations shows that vibrational predissociation has some impact on the electronic predissociation process and affects the final electronic distributions. On the contrary, vibrational product distributions are not significantly affected by the electronic predissociation. A classical description of the ArI_2 dynamics provides an averaged picture of the competing predissociation processes, being better adapted for treating intermolecular vibrational relaxation in the statistical limit. © *2005 American Institute of Physics.* [DOI: 10.1063/1.1832596]

I. INTRODUCTION

Photoexcitation of small van der Waals (vdW) complexes initiates a variety of interesting dynamical processes which occur not only in these weakly bound systems, but also in large molecules and condensed phases. Complexes are therefore often considered as very useful prototypes for understanding the mechanisms of the latter processes in a ''few-atom limit'' and for developing and testing appropriate approaches for their theoretical description. The ArI_2 complex is among the most representative examples exhibiting unexpectedly complicated dynamics. Despite the substantial efforts of several research groups, its understanding still remains full of puzzles and controversies between and among experimental and theoretical results.

Since the state-of-the-art of the problem is presented in a recent review[1] we only sketchily outline here the basic facts and problems which motivated the present study. Throughout the paper, we identify electronic states of the ArI_2 complex through the spectroscopic notations relevant to their precursors in the free I_2 molecule. This classification does not imply that molecular state symmetries are preserved in the complex (see the Appendix).

(i) In its ground electronic state, for brevity $X(0_g^+)$, ArI_2 complex exists in two isomeric forms, linear and *T*-shaped ones, the relative well depth of which is a subject of discussion.

(ii) Excitation to the bound vibrational levels v of the $B(0_u^+)$ state basically gives a continuum for the linear isomer superimposed to discretelike spectrum of broadened peaks corresponding to metastable levels of the *T*-shaped isomer; fluorescence of the $I_2(B,v')$ fragments results from the electronically *adiabatic* vibrational predissociation (VP) process:

$$ArI_2(B,v)\rightarrow Ar+I_2(B,v'). \tag{1}$$

(iii) Fluorescence spectra of the $I_2(B,v')$ fragments show that VP requires a minimum of three vibrational quanta to be transferred from the diatom to vdW bond; closure of vibrational channel at certain initial excitation v allows one to bracket the dissociation energy of the complex.

(iv) Fluorescence quantum yield, relative intensity, total decay rate, as well as the vibrational predissociation efficiency (VPE, the contribution of VP into the total decay rate) are all irregular functions of v, pointing out the existence of concurrent *nonadiabatic* electronic predissociation (EP) process

$$ArI_2(B,v)\rightarrow Ar+2I(^2P_{3/2}), \tag{2}$$

[a]Present and permanent address: Laboratory of Molecular Structure and Quantum Mechanics, Department of Chemistry, Moscow State University, 119992 Moscow, Russia.

which occurs through transitions to weakly bound electronic states crossing the B one; $a'(0_g^+)$, $a(1_g)$, $1(2_u)$, and $B''(1_u)$ states are the most probable candidates for the product EP channels.

One of the most intriguing question is the origin of irregular behavior of the decay rate parameters, especially VPE, which has been accurately measured. Within a kinetic approximation, VPE is given by the ratio of VP rate constant k_{VP} to the total decay rate constant K,

$$\mathrm{VPE}=k_{\mathrm{VP}}K^{-1}=k_{\mathrm{VP}}(k_{\mathrm{VP}}+k_{\mathrm{EP}})^{-1}, \tag{3}$$

so the irregularities may stem from nonmonotonuous variation of both EP and VP rates with v. A possible origin for EP rate oscillations is the *Franck–Condon* (FC) *oscillations* of the probability of discrete-continuum nonadiabatic transition(s) from B to crossing state(s). Oscillations in the VP rate may result from *intramolecular vibrational energy redistribution* (IVR) in a sparse limit, which then proceeds not via the direct coupling to vibrational continuum, but sequentially passing through neighboring metastable levels. Accidental energy resonances or mismatches between these metastable levels introduce irregularities in the VP rate dependence.

Until recently, attribution of VPE oscillations to EP has been predominant. For instance, Burke and Klemperer[2] assumed a smooth dependence of VP rate on v to derive the v dependence of the total rate constants K from the measured VPEs and two rate constant values known from the time-resolved experiments.[3] These results were exploited in several theoretical studies.[4–8] It has also been found that FC oscillations for $B(0_u^+)$-$a(1_g)$ transition can reasonably well fit the measured VPE. However, the theoretical studies on the VP dynamics itself failed to predict smooth variation of k_{VP} with v. Rigorous close-coupling and wave-packet calculations for different potentials and rotational excitations have showed persistent oscillations due to IVR in a sparse-intermediate limit.[9–14] A consistent theoretical treatment of the competition between VP and EP by means of wave-packet propagation on coupled potential energy surfaces (PESs) (Ref. 15) seems to indicate that it is the IVR which manifests itself in the irregular VPE dependence. The primary goal of the present paper is to provide more insight into the competition between VP and EP pathways in the ArI_2 fragmentation dynamics and shed more light on the origin of these VPE oscillations. This is achieved by crossing the results of different computational approaches on this system.

First, we report here on the results of a full wave-packet propagation (FWP) for long enough times such that the dependence of decay branching ratios on excitation energy can be obtained accurately. This improves the quality and supplements the results given in Ref. 15. Second, the bright-state wave-packet (BSWP) approach explored here makes it possible to trace the dynamics after an excitation of each bright state. IVR generally produces an interference between excitation and fragmentation processes owing to intensity borrowing by dark intermediate metastable levels. The overlap of IVR bands belonging to different initial levels v may prevent the definition of state-resolved rates and branching ratios in the FWP calculations, making interesting to separately analyze each band using the BSWP method. Third, it is important to elucidate the role of FC oscillations for different EP channels and the effects of IVR on EP rates. BSWP calculations on the fluxes into each EP channel are supplemented with approximate quantum time-dependent golden rule (TDGR) calculations which provide the EP branching ratios in the limit of no IVR. Fourth, we used quasiclassical trajectory surface leakage (TSL) model to analyze a classical picture of VP/EP competition and demonstrate what factors biased previous theoretical models toward the wrong prediction of FC nature of VPE oscillations. These different methods also provide information on the influence of EP on the VP vibrational product state distributions and thus on a controversy in the experimental determination of the dissociation energy of the complex.

In the following section we survey the theoretical methods used and describe what aspects of the VP/EP competition they describe correctly. In Sec. III such quantities as spectra, VPE, VP product state distributions, and EP branching ratios are considered and compared with available experimental data. In addition, the fragmentation mechanism and the competition between VP and EP channels are discussed. Concluding remarks follow, while some technical symmetry considerations are presented separately in the Appendix.

II. COMPUTATIONAL METHODS

Jacobi coordinates ($\mathbf{R}$,$\mathbf{r}$) are used throughout the paper with $\mathbf{R}$ being the vector joining the I_2 center of mass to the Ar atom and $\mathbf{r}$ the I_2 internuclear vector. The total Hamiltonian has the form (atomic units are used throughout the paper)

$$H=-\frac{1}{2\mu_{\mathrm{Ar,I_2}}}\frac{\partial^2}{\partial R^2}+\frac{\boldsymbol{\ell}^2}{2\mu_{\mathrm{Ar,I_2}}R^2}-\frac{1}{2\mu_{\mathrm{I_2}}}\frac{\partial^2}{\partial r^2}+\frac{\mathbf{N}^2}{2\mu_{\mathrm{I_2}}r^2}+H_{\mathrm{el}}(\mathbf{q}_e;\mathbf{R},\mathbf{r}), \tag{4}$$

where $\mu_{\mathrm{Ar,I_2}}$ and $\mu_{\mathrm{I_2}}$ are reduced masses, $\boldsymbol{\ell}$ and $\mathbf{N}$ are angular momenta associated to $\mathbf{R}$, and $\mathbf{r}$, $H_{\mathrm{el}}(\mathbf{q}_e;\mathbf{R},\mathbf{r})$ is the electronic Hamiltonian, $\mathbf{q}_e$ are electronic coordinates.

The system under study corresponds to a closed shell atom plus an open shell diatomic molecule which obeys Hund case (c) coupling scheme.[16] The total angular momentum of the diatomic fragment is $\mathbf{j}=\mathbf{N}+\mathbf{j}_e$, where $\mathbf{j}_e$ is the electronic angular momentum, orbital and spin.

The ground $X(0_g^+)$ electronic state of the complex is assumed to be isolated from all others so the integration of H_{el} over the electronic coordinates with the corresponding electronic wave function gives a single PES. For describing photodynamics, five electronic states, $B(0_u^+)$, $a'(0_g^+)$, $a(1_g)$, $1(2_u)$, and $B''(1_u)$, are taken into account by constructing 5×5 matrix of H_{el}, but the latter four states are assumed to be coupled only to the B one, not to each other. Diabatic PESs and couplings necessary for parameterization of the electronic part are obtained by means of the first-order diatomics-in-molecule perturbation theory (DIM PT1) (Ref. 17) in its most accurate implementation.[18,19] Exactly the same approach has been used in our previous works.[14,15] The symmetry considerations with respect to parity and permutation symmetries are given in the Appendix.

A. FWP: Full wave-packet method

A FWP method capable to provide ''numerically exact'' description of the photodynamics is used here in the same way as before.[15] The wave packet is expanded as

$$\Psi(\mathbf{r},\mathbf{R},t)=\sum_{j\Omega\omega i}\Phi_{j\Omega\omega i}(r,R)|JM\epsilon_{\Pi}\epsilon_P;\Omega\omega ji\rangle \tag{5}$$

for a given total angular momentum J, its projection M on the space-fixed frame, parity ϵ_{Π} and permutation ϵ_P quantum numbers, as defined in the Appendix. These labels are omitted in the total wave packet designation to simplify the notations. $|JM\epsilon_{\Pi}\epsilon_P;\Omega\omega ji\rangle$ are the symmetry-adapted basis functions defined in Eq. (A3).

The $\Phi_{j\Omega\omega i}(r,R)$ functions are represented on grids and are obtained numerically by integrating the time-dependent Schrödinger equation using a Chebyshev propagator[20] modified by including a damping function in the expansion[21] to avoid reflections. The Hamiltonian matrix elements are expressed in Eq. (A4). The potential term is evaluated by transforming the finite basis set of Eq. (5) to a Gauss–Legendre discrete variable representation.

Initially, the complex is in its ground vibronic level $X(0_g^+)$, $v_X=0$, $n_X=0$ (n_X specifies intermolecular vibrational level in the ground electronic state of the complex; for the B state, index n is used) which corresponds to T-shaped ArI_2 isomer[14,15,18] and rotational level $J=1$, $\epsilon_P=-1$, $\epsilon_{\Pi}=-1$. Dipole excitation promotes the complex into the $B(0_u^+)$ state with $J=0$, $\epsilon_P=-1$, $\epsilon_{\Pi}=1$ (weak continuous absorption to the $B''(1_u)$ state is neglected). Therefore, at time $t=0$ the B-state wave packet is given by

$$\Psi(t=0)=\Psi_B=\langle B(0_u^+)|(\hat{\mathbf{d}}\cdot\hat{\mathbf{e}})|X(0_g^+)\rangle\Psi_{X,v_X,n_X}, \tag{6}$$

where $\hat{\mathbf{d}}$ and $\hat{\mathbf{e}}$ are the dipole moment and photon polarization vectors, respectively, $|B(0_u^+)\rangle$ and $|X(0_g^+)\rangle$ denote the corresponding electronic wave functions.

Practically, Eq. (6) is first projected into the $12\leqslant v\leqslant 28$ subset of the B-state vibrational levels and then discretized on the 200×128 grid in the intervals $[5,25]\times[4.5,9]$ (in atomic units) for R and r, respectively, and expanded over the rotational basis set with maximum I_2 rotational angular momentum 46. Propagation is carried up to 480 ps to reach full convergence of the autocorrelation functions and product populations (previously, only 120 ps limit has been reached and artificial damping has been used to eliminate nonvanishing autocorrelation tails[15]). Fourier transform of the autocorrelation function provides the total absorption spectrum $\sigma^t(E)$. Individual populations of VP products $I_2(B,v',j')$ are evaluated at large R distance as described in Ref. 22 and their half-Fourier transforms provide partial spectra $\sigma^B_{v'j'}(E)$ for each individual rovibrational VP channel.

$a(1_g)$, $B''(1_u)$, $a'(0_g^+)$, and $1(2_g)$ I_2 states are dissociative, and the EP towards these states yields to decay into three fragments, Ar+I+I, Eq. (2). Analysis of the final electronic populations with the flux method, as used for the bound $B(0_u^+)$ vibrational populations, is computationally very inefficient, since it involves the integration over the relative kinetic energy of the I+I fragments. The final distributions of dissociative electronic states is more easily computed using the BSWP method described below.

B. BSWP: Bright-state wave-packet method

Total absorption spectrum obtained in the FWP calculations provides converged results over the energy region covering vibrational bands of the complex $15\leqslant v\leqslant 25$. It shows groups of peaks readily assignable to particular (v,n) metastable levels:[14,15] IVR gives rise to the appearance of weak additional spectral features corresponding to the absorption of intermediate dark metastable states populating in the course of VP through intensity borrowing.[14,15] These groups of peaks, or IVR bands, in principle cannot be rigorously assigned, especially if they overlap.

In order to check approximate assignment of each IVR band, which is necessary for the state-resolved analysis of the decay dynamics, a BSWP method is applied. It is formally the same as FWP, except that the initial wave packet is given by a zero-order bound-state approximation of the excited bright metastable state

$$\Psi(t=0)=\Psi_{B,v,n}=\chi_v^B(r)\Phi_{B,v,n}(R,\theta). \tag{7}$$

Therefore, BSWP calculations are to be made for each v, n band separately to produce the corresponding IVR band. The sum over the BSWP spectra over all v, n with the weights given by expansion coefficients of Ψ_B (6) onto $\Psi_{B,v,n}$ set (7) is formally equivalent to the FWP spectrum up to the interference effects in overlapping IVR bands. Hence, FWP and BSWP calculations are complementary. The first one allows to calculate at once the whole spectrum and obtain the magnitudes discussed above. The final FWP propagation time corresponds to the slowest process. On the contrary, using BSWP method one single propagation (but perhaps for shorter times) must be performed for each initial v, n couple, which is less efficient. The advantage, however, is that BSWP method makes possible a direct state-resolved analysis of the energy flux among the different degrees of freedom, thus providing a deeper physical insight on the process under study. Parameters of the numerical implementation of the BSWP method are chosen to achieve close convergence with the spectra obtained within FWP method.

C. TDGR: Time-dependent golden rule method

More drastic simplification can be attained assuming that EP, which proceeds on the strongly repulsive PESs, is *faster and independent* from VP. Thus, initially excited bright state decays through EP to each individual crossing state α so fast that the Ar atom has no time to move acting merely as a ''spectator.'' In this case EP dynamics can be treated perturbatively within the TDGR approximation.[6] Wave packet is represented by

$$\Psi(t=0)=\Psi_{\alpha,v,n}=V_{B\alpha}\Psi_{B,v,n}, \tag{8}$$

where $\Psi_{B,v,n}$ is given by Eq. (7) and $V_{B\alpha}$ is the diabatic coupling between the final α electronic state and the B state. The propagation is carried out on the single PES of the α state. Note that as far as the TDGR neglects all the interference effects between the VP and EP, as well as among dif-

ferent EP channels, it reduces the problem to a kinetic description with the partial EP rate constant k_{EP}^{α} given by[23]

$$k_{\mathrm{EP}}^{\alpha}=\frac{1}{2\hbar^2}\int_{-\infty}^{+\infty}dt e^{iE_{vn}t}\langle\Psi(t=0)|\Psi(t)\rangle, \tag{9}$$

where E_{vn} is the energy of the initial bright state in Eq. (7). The wave packet is represented in a grid composed of 80 Gauss–Legendre points in θ, 90, and 1024 equidistant points in the intervals [2.5,10] and [2.2,8] Å for r and R coordinates, respectively. The convergency is reached at times as short as 100 fs, and a small time step of 0.1 fs is used.

D. TSL: Trajectory surface leakage model

The competition between VP and EP channels can be also considered using the classical description of the vibrational dynamics of the complex. This is done within the TSL model introduced in Ref. 7. In brief, the trajectories are propagated on the B-state PES until the VP will occur, as monitored by the standard approach, see, e.g., Ref. 24. However, each time the trajectory passes through the crossing seam between the B and one of the repulsive state α, the probability of EP is calculated by the standard Landau–Zener formula[25,26]

$$p_{\alpha}=1-\exp\left[-2\pi\frac{V_{B\alpha}^2(\mathbf{q}_c)}{\hbar g(\mathbf{q}_c)|F_B(\mathbf{q}_c)-F_{\alpha}(\mathbf{q}_c)|}\right], \tag{10}$$

where $\mathbf{q}_c$ are the coordinates of the point at the crossing seam, g is the velocity component orthogonal to the crossing seam, and F_B, F_{α} are the slopes of diabatic potentials at the crossing point. The probability of EP to each state α is accumulated along the trajectory, whereas its weight is reduced by the corresponding quantity.

Batches of 250 trajectories are propagated for each v up to 300 ps. Initial quasiclassical conditions are selected randomly for the energies corresponding to bright states (7) with $n=0$. VP and EP probabilities as the functions of time are accumulated and used to determine the corresponding rates and branching ratios.

III. RESULTS

A. Spectra and vibrational predissociation efficiencies

The structure of the total photon absorption spectrum $\sigma^t(E)$ is determined by excitations of different $I_2(B,v)$ vibrational levels within the complex. It consists of narrow bands, the energies of which have a clear systematics. Because the vdW potential of the initial $ArI_2(X)$ state is very similar to that of $ArI_2(B)$ state in the vicinity of the T-shaped potential well,[14,18] the Franck–Condon factors favor excitations with the same vdW excitation n. For this reason absorption to $n=0$, 1, and 2 was detected experimentally[2,27] with decreasing intensity when increasing n. In close agreement with experiment, the bands in the theoretical spectrum cluster in groups of three members, the low energy one being more intense and the second and third being 24 and 30 cm^{-1} higher in energy than the first one.[14] Band clusters are separated from each other by the vibrational energy spacing of

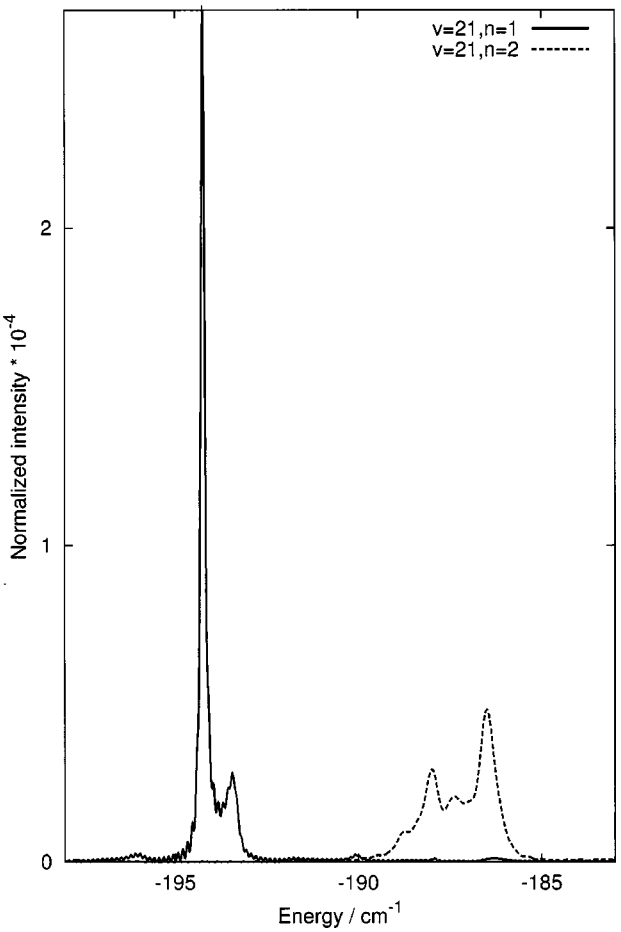

FIG. 1. Absorption spectrum calculated using the BSWP method for $v=21$ and $n=1$, 2 bands.

$I_2(B)$. This systematic allows to assign approximate I_2 stretching v quantum number to each cluster and classify each band within it as the excitations of ArI_2 vdW bending-stretching levels $n=0-2$ (Refs. 14 and 27). Typical structure of IVR bands as obtained with the BSWP method is exemplified for $v=21$ and $n=1$, 2 in Fig. 1. It shows that each band usually contains several overlapbing lines. For $n=0$ (not shown) and $n=1$, there are usually one central line, which is the most intense, and two satellite ones, which are weaker. For $n=2$, the band structure is usually more complicated. This has been interpreted as the result of interaction between the levels of different stretching manifolds through IVR,[14,15,28] as discussed further in Sec. III D.

The total photon absorption spectrum $\sigma^t(E)$ includes the contributions from both VP [partial cross section $\sigma^B(E)$], which can be detected experimentally through fluorescence of the product $I_2(B)$ molecule, and EP, which corresponds to dark channels. For a given IVR band v, n, the vibrational predissociation efficiency $\mathrm{VPE}(v,n)$ is defined as

$$\mathrm{VPE}(v,n)=\frac{I^B(v,n)}{I^t(v,n)}, \tag{11}$$

where $I^B(v,n)$ and $I^t(v,n)$ refer to the band intensities obtained by integration of the spectra $\sigma^B(E)$ and $\sigma^t(E)$

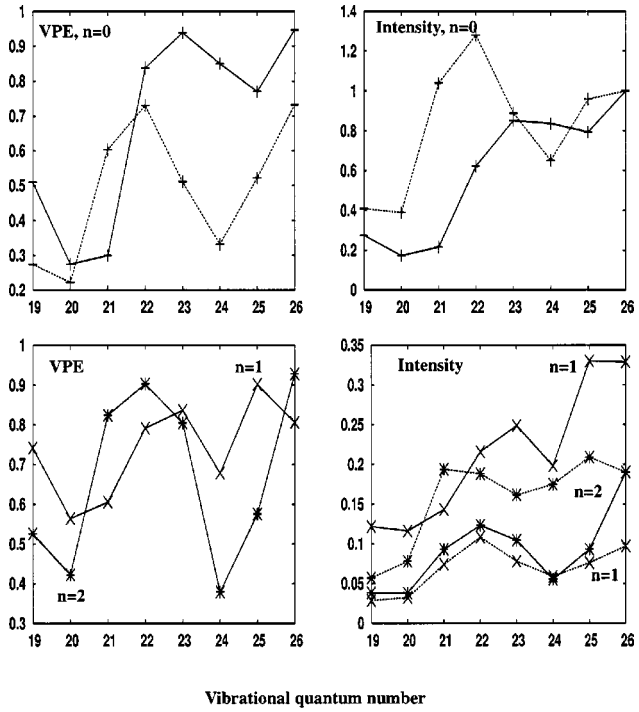

FIG. 2. Left: vibrational predissociation efficiency for different initial vibrational excitation v. Right: Relative fluorescence intensity for the same excitations. Top: no initial vdW excitation ($n=0$). Bottom: first ($n=1$) and second ($n=2$) vdW excited bands. Full lines correspond to FWP computational results, dashed ones to the experimental results from Burke and Klemperer (Ref. 2). Intensities are normalized so that they are unity for $v=26$, $n=0$. An additional normalization is used for the experimental results for $n=1$, 2, so that calculated and measured relative intensities coincide for $v=26$, $n=2$.

$$I^B(v,n)=\int_{bw(v,n)}\sigma^B(E)dE,$$

$$I^t(v,n)=\int_{bw(v,n)}\sigma^t(E)dE \tag{12}$$

over the bandwidth $bw(v,n)$ which covers the whole IVR band. This bandwidth depends on the band considered but is typically of the order of one wave number. Thus I^B represents the total fluorescence intensity of the band. The dependences of $I^B(v,n)$ and VPE(v,n) on v for three excitations $n=0-2$ obtained with FWP method are shown in Fig. 2 together with available experimental data.[2] VPE can also be obtained using the BSWP method, and it was checked that both methods agree with each other very well, indicating that overlapping between adjacent bands is negligible. In this situation FWP and BSWP calculations are equivalent.

Agreement between calculations and experiments is qualitatively good: both VPE and I^B generally increase, but at the same time oscillate with v. The overall increase is a consequence of the growing VP contribution due to the decreasing energy gap. Increase of intensities is further enhanced by the B-X excitation FC factor, which grows up in this energy region. Oscillatory behavior is very pronounced for both VPE and intensities. Calculated dependences are qualitatively similar for the three excitations $n=0-2$, all having two minima at $v=20-21$ and at $v=24$, and at least one maximum at $v=22-23$. Measured quantities show quite similar pattern although the positions of their features can be shifted by one vibrational quantum.

The major disagreement between theory and experiment is the opposite intensities for excited $n=1$ and $n=2$ bands. Indeed, calculated $I^B(v,n=1)$ curve is close to measured $I^B(v,n=2)$ one and vice versa. This artifact can be explained either by some inaccuracy of the B-state interaction potential or by overall rotational excitation in the measured spectrum. The zero-order wave functions of $n=1$, 2 levels do not show clear stretching-bending nodal patterns and should be considered as a Fermi diad separated by 7 cm^{-1}.[14] Small variation of the interaction or centrifugal potential can therefore easily invert the wave function and intensity patterns.

Previously, we have estimated VPE for $n=0$ band in a kinetic approximation (3) combining k_{VP} from the separate calculations without EP and total decay rate constant K from low-resolution FWP calculations.[15] Such a definition is rather crude, but unambiguously points out VP as the source of VPE oscillations. The fact that present accurate calculations give essentially the same VPE (cf. Fig. 2 here and Fig. 8 in Ref. 15) supports the kinetic approximation. We will come back to this interpretation later on in Sec. III D.

Close similarity in fluorescence intensity patterns for different n bands is symptomatic. Klemperer and co-workers[2] interpreted it as a signature of IVR in statistical limit, where VP rate oscillations do not occur. Later, it was discussed that such similarity could be due to the mixing of the states associated to $n=1$ and 2, which are only separated by few wave numbers and would interact among them, thus sharing the dynamical features.[15] Present calculations, however, show (see, for instance, Fig. 1 for $v=21$) that the intensity sharing between the two bands is negligible. However, the initial states for $n=1$ and 2 correspond to a Fermi diad thus sharing the nodal structure. Although the structure of $n=1$ and especially $n=2$ IVR bands is more complicated than that of $n=0$ band indicating that more dark states are involved in IVR, it does not reach the statistical limit. It may be suggested that the spacing between excited vdW levels only slightly varies with v so that the dark levels of the same nature are involved in IVR in each v manifold.

B. Vibrational product state distributions

Table I compares product vibrational distributions for VP of $ArI_2(B,v,n=0)$ with available experimental results from Johnson, Sharfin, and Levy.[29] In addition to FWP data, TSL results are also presented. In order to assess the influence of EP on the vibrational dynamics, both methods are implemented in two versions, with and without inclusion of EP. There is a good agreement between both calculation methods and experiment. The distribution always has a maximum for the first open vibrational channel $\Delta v=-3$.

It was suggested that EP quenching efficiency may increase with vibrational excitation of $I_2(B)$ products.[30] With less translational energy available, Ar will recoil more slowly from vibrationally excited I_2, leaving more time for quenching by EP to occur and producing significant reduction of the population of the highest VP channels. This argument was

TABLE I. Vibrational product state distributions $I_2(B,v')$ for three different initial excitations $v=16$, 21, and 24 of the $ArI_2(B)$ complex. The results of two FWP and TSL calculations are presented, without (no EP) and with inclusion of EP. Experimental data are from Ref. 29.

	v'	TSL, no EP	FWP, no EP	TSL	FWP	Expt.
	11	0.01	0.00	0.01	0.00	⋯
$v=16$	12	0.08	0.21	0.08	0.21	0.13
	13	0.91	0.79	0.91	0.79	0.87
	15	0.00	0.02	0.00	0.01	0.01
$v=21$	16	0.03	0.05	0.03	0.04	0.03
	17	0.24	0.15	0.24	0.15	0.16
	18	0.73	0.78	0.73	0.80	0.79
	17	0.00	0.01	0.00	0.00	⋯
	18	0.01	0.04	0.01	0.04	⋯
$v=24$	19	0.10	0.11	0.09	0.10	0.07
	20	0.24	0.25	0.25	0.25	0.21
	21	0.65	0.58	0.65	0.59	0.72

necessary to support the indirect estimate of the $ArI_2(B)$ dissociation energy derived from the dissociation energy of linear $ArI_2(X)$ isomer by means of relative absorption intensity and excitation blueshift analysis.[30] The resulting value $D_0(B)=128\,cm^{-1}$ appeared to be markedly smaller than that obtained from threshold effects in the vibrational distributions $D_0(B)=223\,cm^{-1}$.[31] With the former smaller dissociation energy, the VP channel $\Delta v=-2$ is open in the excitation energy range considered here, and in order to explain why no associated fluorescence is observed, one has to assume its nearly 100% quenching by EP.[30] Our results demonstrate that such a high quenching efficiency is very unlikely. In fact, the time during which Ar and I_2 remain in close contact so that quenching can occur is merely the lifetime of the $ArI_2(v,n)$ resonance, which is independent of the product channel which the system eventually chooses. Moreover, essentially classical arguments of Ref. 30 are not supported even by the quasiclassical TSL model. In a classical interpretation, the difference in available translational energy is important only out of the interaction region where the quenching rate is negligible due to rapidly vanishing nonadiabatic coupling. We therefore conclude that the older dissociation energy from Blazy *et al.*[31] is more grounded, all the more as it has been also confirmed by more recent rotationally resolved measurements of the product state distributions.[32] As has been argued in our previous work,[15] the most probable origin of discrepancy is the inherent difficulty of quantitative separation of absorptions by *T*-shaped and linear isomers and evaluation of their relative populations. Notice, however, that the present discussion does not question the energetics of linear isomer in the *X* state, directly established by Klemperer and co-workers.[30]

C. Electronic predissociation branching ratios

EP branching ratios as the functions of v are shown in Fig. 3. We discuss first the BSWP results depicted in panels *a*, *c*, and *d* for for $n=0$, 1, and 2, respectively. The $B''(1_u)$ population is the lowest and increases monotonuously with v for all three vdW excitations, while $a(1_g)$, $a'(0_g^+)$, and

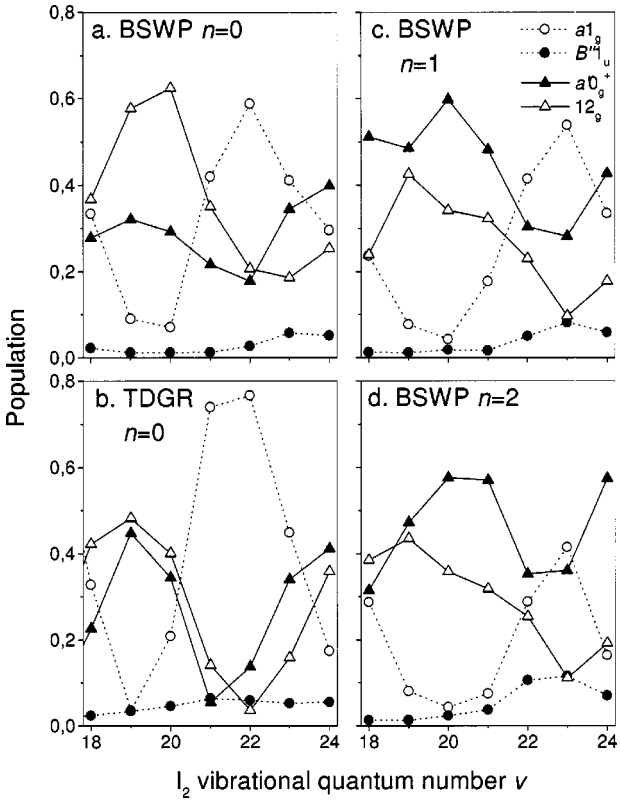

FIG. 3. Final populations of the different EP channels as the functions of the initial $I_2(B,v)$ excitation. Panels (a), (c), and (d) represent BSWP results for $n=0$, $n=1$, and $n=2$, respectively, panel (b) shows TDGR result for $n=0$. The sum of probabilites is normalized to 1.

$1(2_g)$ distributions show oscillatory patterns similar for all three values of *n*, by reasons which will become clear below. The major difference concerning excitation of the vdW modes is the relative importance of each electronic state: the $a(1_g)$ state population seems to be independent of the initial excitation *n*, while for $a'(0_g^+)$ and $1(2_g)$ there is an inversion when increasing vdW excitation from $n=0$ to $n=1$ and 2.

The difference between the different vdW levels is that $n=0$ corresponds to the ground level with a maximum distribution at *T*-shaped configuration, while $n=1$ and 2 levels are a diad showing a combined stretching-bending nodal structure (see Fig. 4 in Ref. 14), with the distribution thus shifted away from the *T*-shaped configuration. Therefore, the differences among the electronic distributions should be related to the topology of the electronic couplings.

Among the couplings between the *B* and all crossing states, only that with $a(1_g)$ state is symmetric with respect to permutation of iodine nuclei and does not vanish at strictly *T*-shaped configuration ($\theta=\pi/2$). Thus, the coupling between the *B* and $a(1_g)$ states do not vary significantly when promoting from $n=0$ to $n=1$ and 2. In fact, there is a small overall decrease in the final $a(1_g)$ probability for the excited vdW levels, and a change in the maximum with v probably due to the energy shift involved.

All other electronic couplings vanish for $\theta=\pi/2$, but grow up if θ deviates from the right angle. In such nonsymmetric configurations, the average magnitude of the coupling

with $a'(0_g^+)$ state is the largest, while that with $B''(1_u)$ state is the smallest, so that $a'(0_g^+)$ becomes nearly predominant for both $n=1$ and 2, while $B''(1_u)$ distribution only increases a little. The reason why the $1(2_g)$ ratio seems to decrease when increasing n could be explained by the large increase of the $a'(0_g^+)$ probability. With this argument, it is also clear why the $a'(0_g^+)$ and $1(2_g)$ relative contributions are very similar for the two excitations, $n=1$ and 2. The origin of the oscillatory patterns with v should now be interpreted.

EP branching ratios obtained using BSWP method are affected by the full complexity of the VP dynamics. It is interesting to compare them with the results of a crude zero-order approximation, assuming that EP is essentially due to the bright state. Initially populated bright state undergoes fragmentation following two alternative and almost independent pathways: the first involves IVR-mediated VP mechanism, the second direct EP towards the dissociative electronic states. The EP dynamics can be studied independently for each final channel using the TDGR method explained above.

EP branching ratios calculated within the TDGR method for $n=0$ are presented in panel (b) of Fig. 3. Although oscillatory patterns are qualitatively similar to those obtained with BSWP method [panel (a)], there are some differences. First, TDGR overestimates the contribution of the $a(1_g)$ EP channel. This is a consequence of the bright-state approximation. As has been mentioned above, $n=0$ bright state is localized in the vicinity of *T*-shaped minimum where it is coupled to the $a(1_g)$ channel only. The dark states involved in IVR originate from highly excited vdW zero-order levels, which, due to delocalization in deformation angle, are more efficiently coupled to other EP channels. Second, the shapes of the TDGR branching ratios are very similar to the oscillatory patterns of the FC factors between the bright state and isoenergetic continuum functions of the crossing electronic states, e.g., the former drops almost to zero at the excitations where FC factors vanish. BSWP method gives more smoothly varying branching ratios which do not vanish at these points. Again, it reflects the contribution of the dark states, whose FC factor with the EP continuum functions should be different. Moreover, the BSWP branching ratios further depart from FC factor dependence if n increases as a consequence of the growing density of dark states.

The similar v-dependence of the partial EP rates, defined within the TDGR method, and the electronic branching ratios, obtained with the BSWP method, allow us to attribute the origin of the appeareance of the oscillations to FC factors.[4] It was also found that the necessary condition for this oscillation to persist when taking into the dissociation dynamics is the spectator behavior of Ar atom within the complex.[5,6] This, in turn, can take place only if the interaction potential of the repulsive electronic states is bound along the radial vdW coordinate. Previously, this fact was used to obtain a semiempirical guess to $a(1_g)$ vdW potential.[5,6] Present DIM PT1 model reproduces the vdW potential wells naturally, thus providing extra support to the predictions made within a spectator model.

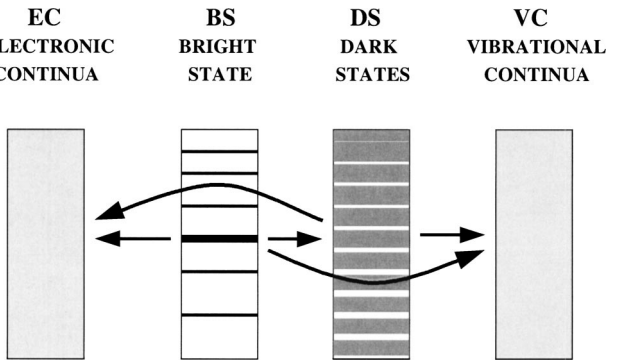

FIG. 4. Schematic representation of the ArI_2 fragmentation mechanism through EP and VP channels.

D. Analysis of fragmentation dynamics

The fragmentation dynamics is nonexponential, as shown by the non-Lorentzian shape of the spectra, in Fig. 1, because of the IVR in the sparse-intermediate regime. It is, however, convenient to define approximate rate constants of the various processes contributing to overall decay in order to gain more insight into the fragmentation mechanism, considering the evolution of the population in time and interpreting it within suitable kinetic models.

Schematic picture of the fragmentation process is presented in Fig. 4. Initially excited bright state v, n (BS) is coupled to the electronic continua (EC) of the dissociative electronic states by the diabatic couplings, which cause EP, and to vibrational continua (VC) with $v'<v-2$ due to vibrational couplings, which cause direct VP. Much stronger vibrational couplings, however, link BS to the dark states (DS) belonging to $v'=v-1$, $v-2$ manifolds. The latter, in turn, are also coupled to electronic and vibrational continua. This picture is merely a generalization for EP of the analytical model elaborated previously.[28] Operating with three effective parameters, Δ for the spacing between the dark states, Γ for the width of the dark states, and V_{bd} for the coupling between BS and DS manifolds, this model allowed to distinguish the limits of no IVR ($\Gamma \ll \Delta$) and statistical IVR ($\Gamma \gg \Delta$), as well as the intermediate case of sparse IVR ($\Gamma \approx \Delta$), and characterize their signatures in the spectral profiles and evolution of populations in time.[28] In terms of this model, the VP dynamics of the ArI_2 complex in the absence of EP was analyzed.[10,11,14] Inclusion of EP in the model makes it analytical solution cumbersome, but it still can be used for qualitative interpretation.

Similarity of the FWP and BSWP spectra reveals that bright states v, n keep their identity in the absorption (i.e., statistical limit of IVR is not reached). The coupling to the DS manifold manifests itself in the appearance of weak satellite features in each band. For $n=0$ and $n=1$ bands, typically two such features appear (see Fig. 1 for the latter case). According to IVR model, this indicates that at least two dark states are involved, in agreement with the sequential three-quantum energy transfer in the VP process.[10,11,14] For $n=2$, the band structure is typically more complicated (Fig. 1), indicating enhancement of IVR due to larger DS density. As has been shown previously,[15] EP does not affect the spectra

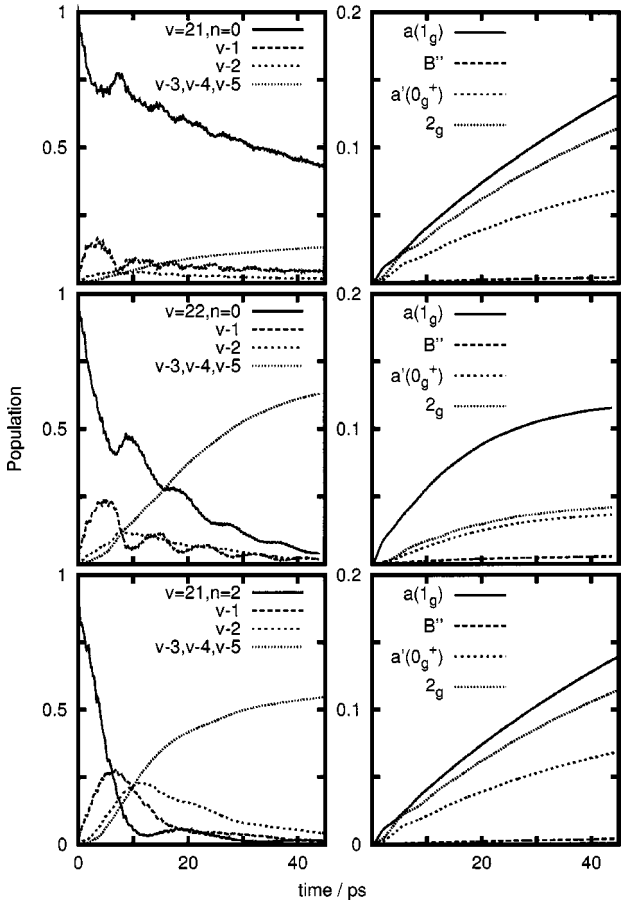

FIG. 5. Vibrational (left panels) and electronic (right panels) populations vs time obtained in the BSWP method for $v=21$, $n=0$ (top), $v=22$, $n=0$ (middle), and $v=21$, $n=2$ (bottom).

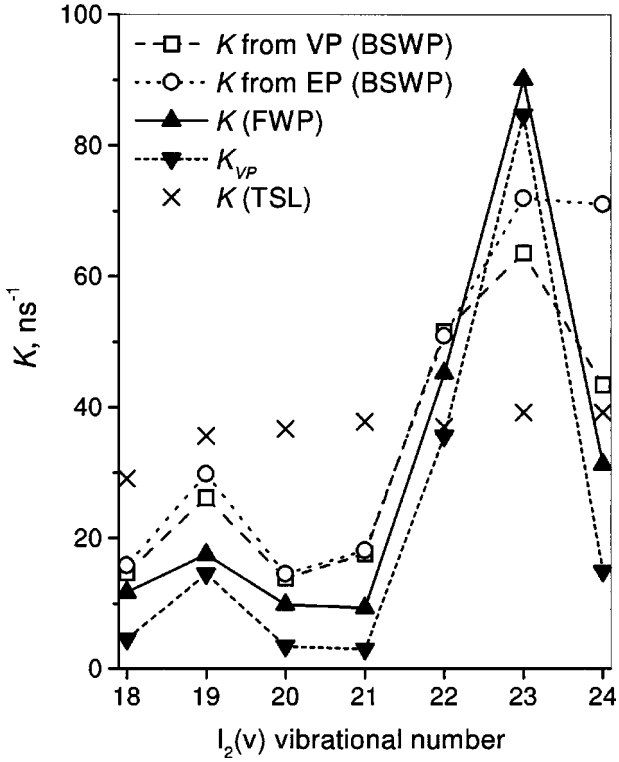

FIG. 6. Total decay rates K obtained for different I_2 vibrational excitations, but for the same ground vdW level $n=0$, from different methods. For BSWP, exponential fits of the time dependence of either VP or EP product populations have been made. A similar procedure has been used for TSL. For FWP, photon absorption spectra have been fitted to Lorentzians. Also shown is the VP rate, obtained in a FWP calculation where EP channels are not included.

except making the bands broader, because the electronic states responsible for the EP are dissociative with no bound or quasibound levels.

Figure 5 exemplifies the time evolution of vibrational and electronic populations for $v=21$, $n=0$, $v=22$, $n=0$; and $v=21$, $n=2$ from the BSWP calculations. The decay of BS and transients corresponding to $v-1$ and $v-2$ DS manifolds have oscillatory behavior, a clear signature of IVR in a sparse limit.[28] Oscillation intensity and period reflect the ''amount'' of IVR, i.e., the contribution of the sequential BS→DS→VC vibrational predissociation pathway. The case $v=21$, $n=0$ corresponds to slow VP with little IVR: the weak beats occur over an almost exponential decay typical of direct BS→VC mechanism. The case $v=22$, $n=0$ exhibits more pronounced role of IVR which facilitate the VP process. Finally, for $v=21$, $n=2$ the first IVR oscillation becomes rate limiting. This case is not far from the statistical IVR limit, when the decay exponent is determined by the DS→VC rate because the bright state is completely dissolved in the DS quasicontinuum.[28]

In contrast, the populations of EC and VC manifolds closely follow exponential accumulation law

$$Q_\alpha(t)=A_\alpha[1-\exp(-Kt)], \tag{13}$$

valid for the decay into several independent channels α. The total decay rate constants K for $n=0$ obtained by fitting the populations of EC and VC manifolds to Eq. (13) are compared in Fig. 6 with the total rate determined from the bandwidths in the FWP calculations and the VP rate k_{VP} computed in the absence of EP.[14,15] Agreement between the results of the fit is good, except for the highest v's, indicating that EP and VP channels can be considered as independent. The discrepancies between the fits from VP product and EP product at high v may be the fingerprint of the breakdown of the exponential kinetic laws when IVR becomes important in VP. Figure 6 shows a striking similarity between FWP total rates and VP rates. This shows that EP does not affect the VP process significantly. The same conjecture follows from the similarity of the vibrational product distributions obtained with and without EP (see Table I).

The influence of the VP process on the EP rate can be estimated by comparing FWP or BSWP results with TDGR ones. TDGR calculations for $n=0$ provide an estimate of EP rates in the absence of VP. The sum over the oscillating rates for each decay channel is essentially constant: EP rate varies within the interval 4.6 to 7.2 ns^{-1}, much smaller than the variation of K and k_{VP} rates depicted in Fig. 6. This strongly supports the conclusion that large oscillation in the VPE should be attributed to IVR, not to FC oscillations in the EP rate. Crude estimation of the EP rate as the difference of the total decay rates obtained in FWP calculations with and without VP (Refs. 14 and 15) gives irregular dependence with the average value of 10 ns^{-1}. It is likely that IVR affects the EP

TABLE II. Averaged branching ratios for different EP channels calculated using TDGR, TSL, FWP, and Landau–Zener fast and slow models (see text for explanation).

State	FWP[a]	TDGR	TSL	LZ fast	LZ slow
$a(1_g)$	0.19	0.45	0.13	0.36	0.05
$a'(0_g^+)$	0.46	0.19	0.50	0.32	0.65
$B''(1_u)$	0.04	0.01	0.04	0.02	0.11
$1(2_g)$	0.31	0.34	0.34	0.30	0.19

[a]Reference 15.

rate mainly changing the branching ratios between distinct EP channels, as has been discussed in the preceding section.

It is interesting to study what aspects of this predissociation mechanism can be retained by classical description within the TSL model. Being considered in terms of the phase-space classical dynamics, VP corresponds to the drift of phase points along the stochastic component of the phase-space region where the bound complex exists. Eventually, phase points reach the separatrix and escape to the unbound portion of the phase space.[35] Therefore, TSL model can be viewed as describing IVR in the statistical limit. In the scheme shown in Fig. 4, TSL model does not distinguish BS and DS manifolds, which both correspond to the phase-space region where the bound complex exists. In addition, EP is simulated along the long-lived trajectories with thousands of successive passages through the crossing seams, which produce a small incremental growth of the EC population in time. FC oscillations occurring in the quantum treatments of the EP are not taken into account. As a result, TSL gives smoothly varying rates and branching ratios.

As far as the model of independent decay channels is strictly valid for classical description, all partial rates can be determined using Eq. (13) from the populations in particular decay channels. All give the same total rate K (within the statistical error) and partial rates as $A_\alpha K$. Total decay rate slowly grows up with v, as shown in Fig. 6, representing ''an average'' over the IVR oscillations in the quantum rates. Increasing component is k_{VP}; k_{EP} slightly decreases from 12.5 to 8 ns^{-1}, being also close to the ''average'' quantum EP rate.

EP branching ratios are essentially independent on v. They are given in Table II together with other averaged estimations. TDGR estimation is obtained by dividing TDGR rates for $n=0$ by appropriate FC factors with the continuum functions and averaging over v; FWP result was obtained in Ref. 15 from the short-time wave-packet propagation. In addition, two simple quasiclassical Landau–Zener (LZ) estimations are presented. The ''fast'' one is equivalent to a bright-state approximation and is obtained by averaging LZ formula (10) over R and θ with the $\Phi_{B,v,n}(R,\theta)$ bright-state wave function (7). The ''slow'' one is the average over the whole configuration space in R and θ variables.

Classical bright-state approximation (LZ fast) agrees with the quantum one (TDGR) in the predominance of $a(1_g)$ channel open in the T-shaped geometry. It overweights, however, $a'(0_g^+)$ channel, the most efficient for bent configurations. Indeed, if the VP is slow and the system has time to explore the whole configuration space (LZ slow), decay through $a'(0_g^+)$ state is clearly dominant. Actual TSL results are in between of two LZ extremes, being closer to the slow one. They are also very similar to quantum FWP data which corresponds to the fluxes averaged over the whole absorption spectrum.[15]

Although the branching ratios presented in the Table II are rather approximate due to distinct way and degree of averaging for different methods, they point out that classical description is able to provide reasonable ''coarse-grained'' picture of the process. It is expected to be more accurate once true quantum dynamics approaches the statistical limit. In the sparse IVR regime considered here, classical mechanics inherently neglects quantum effects, which are responsible for oscillatory behavior of both EP and VP probabilities. Serious caution must be taken when using the hybrid approaches. For instance, the method used to describe ArI_2 fragmentation in Ref. 8 takes into account the FC oscillations in the EP channel, but describes vibrational dynamics classically neglecting the oscillations due to IVR. Its results are therefore biased toward the wrong attribution of oscillations in the VPE and total rate to EP.

IV. CONCLUSIONS

We have used quantum and classical methods to study the fragmentation dynamics of the ArI_2 van der Waals complex where both vibrational and electronic predissociation mechanisms are allowed to compete. We have produced such quantities as the partial and total absorption spectra, vibrational, and electronic product state distributions for a large range of I_2 and van der Waals vibrational excitations, and compare them, whenever possible, with experimental data. The main finding can be summarized as follows.

(i) Oscillating behavior of the measured vibrational predissociation efficiencies is well reproduced using accurate full and bright-state wave-packet methods implemented on the coupled potential energy surfaces. The main source of these oscillations is the IVR in a sparse-intermediate limit affecting vibrational predissociation dynamics, not the Franck–Condon oscillations of the electronic predissociation probability.

(ii) The reason why the latter do not produce major effect on VPE is the coexistence of three distinct EP channels, namely, $a(1_g)$, $a'(0_g^+)$, and $1(2_g)$. The EP probabilities for each state do exhibit FC oscillations, but they tend to cancel each other in the total EP probability.

(iii) The influence of EP channel on the VP dynamics is minor, while VP affects the EP branching ratios by virtue of spreading the wave packet in the bending angles due to IVR involving bending-excited dark states.

(iv) Classical description is valid for IVR in the statistical limit. In the present case it can give only averaged picture of the process.

(v) Vibrational product state distributions are not affected by EP. The latter process is unlikely responsible for quenching of the $v-2$ VP channel. This conclusion supports the early experimental estimation of the $ArI_2(B)$ dissociation energy $D_0=223\,\mathrm{cm}^{-1}$.[31]

These conjectures have been obtained by using several dynamical methods on a single set of semiempirical DIM

TABLE III. Action of the parity and permutation operators on the basis functions.

	φ_R	θ_R	φ_r	θ_r	$D^{J*}_{M\Omega}(\varphi_R,\theta_R,\varphi_r)$	$D^{j*}_{\Omega\omega}(0,\theta_r,0)$	$\phi_e^{\omega i\sigma}$
Π	$\pi+\varphi_R$	$\pi-\theta_R$	$\pi-\varphi_r$	θ_r	$(-1)^{J+\Omega}D^{J*}_{M-\Omega}$	$D^{j*}_{\Omega\omega}$	$\sigma\phi_e^{-\omega i\sigma}$
P	φ_R	θ_R	$\pi+\varphi_r$	$\pi-\theta_r$	$(-1)^{\Omega}D^{J*}_{M\Omega}$	$(-1)^{j+\Omega}D^{j*}_{\Omega-\omega}$	$i\sigma(-1)^{\omega}\phi_e^{-\omega i\sigma}$

PT1 potential energy surfaces. It would be interesting to assess the quality of the potentials used here further, for instance by comparison with *ab initio* calculations. It would then be useful to study the sensitivity of the present findings on modifications of the potentials. Work along this line is currently in progress.

ACKNOWLEDGMENTS

The authors thank A. Beswick and N. Halberstadt for useful discussions. An allocation of CPU time on the NEC SX-5 vector computer of the ''Institut du Développement et des Ressources Informatiques Scientifiques'' is gratefully acknowledged. The authors also wish to acknowledge a CNRS-CSIC, Grant No. 2004FR0003, for supporting travel expenses between Toulouse and Madrid. A.A.B. acknowledges Paul Sabatier University for Invited Professor fellowship and Russian Fund of Fundamental Research for financial support (Project No. 02-03-32676). O.R. thanks Ministerio de Ciencia y Tecnología, Spain, for financial support under Grant No. BFM2001-2179.

APPENDIX: SYMMETRY OF ELECTRONIC AND NUCLEAR WAVE FUNCTIONS

We consider a triatomic AB_2 (ArI_2) system where two of three atoms are identical. We further assume the electronic states to result from the interaction between a closed shell ^1S state of atom A with the states of B_2 molecule which obey Hund case (c) coupling scheme. We show in this Appendix how to build up the total electronic-nuclear wave functions with the correct parity and permutation symmetries in this case.

1. Frames, symmetries, and basis functions

Let (θ_R,φ_R) be the spherical polar coordinates of $\mathbf{R}$ in the space-fixed (SF) frame $(\mathbf{I_L},\mathbf{J_L},\mathbf{K_L})$. An atom-diatom molecular body-fixed (BF) frame $(\mathbf{I_R},\mathbf{J_R},\mathbf{K_R})$ is associated to Euler angles $(\varphi_R,\theta_R,0)$ such that

$$\mathbf{K_R}=\mathbf{R}/|\mathbf{R}|,\quad \mathbf{J_R}=\mathbf{K_L}\times\mathbf{R}/|\mathbf{K_L}\times\mathbf{R}|,\quad \mathbf{I_R}=\mathbf{J_R}\times\mathbf{K_R}. \tag{A1}$$

Let (θ_r,φ_r) be the spherical polar coordinates of $\mathbf{r}$ in this frame. The diatom molecular frame (MF) $(\mathbf{I_r},\mathbf{J_r},\mathbf{K_r})$ is associated to Euler angles $(\varphi_r,\theta_r,0)$ so that

$$\mathbf{K_r}=\mathbf{r}/|\mathbf{r}|,\quad \mathbf{J_r}=\mathbf{R}\times\mathbf{r}/|\mathbf{R}\times\mathbf{r}|,\quad \mathbf{I_r}=\mathbf{J_r}\times\mathbf{K_r}. \tag{A2}$$

Let $\mathbf{J}$ be the total angular momentum, which results from the addition of the atom-diatom ℓ and diatom $\mathbf{j}$ angular momenta. $\mathbf{j}$ in turn results from the addition of the rotational angular momentum $\mathbf{n}$ and of the total (orbital plus spin) electronic angular momentum $\mathbf{j}_e$. The common projection of $\mathbf{J}$ and $\mathbf{j}$ on the $\mathbf{K}_R$ axis is called Ω, and the common projection of $\mathbf{j}$ and $\mathbf{j}_e$ on $\mathbf{K}_r$ is ω.

Because atom A is in a closed-shell spherically symmetric state, diabatic electronic states $\phi_e^{\omega i\bar{\sigma}}$ for the triatomic system can be labeled by the quantum numbers of the isolated B_2 molecule.

(1) ω the electronic angular momentum projection on $(\mathbf{K_r})$, which we assume integer.

(2) $i=\pm$, the effect on the *electronic* wave functions of the inversion of electronic coordinates in the fixed molecular frame $(\mathbf{I_r},\mathbf{J_r},\mathbf{K_r})$. This operation is denoted as $\mathbf{i}$ and corresponds, in spectroscopic notations, to the g/u character of the state.

(3) $\sigma=\pm1$, such that the effect of the symmetry through the triatomic molecular plane $\sigma_v(I_rK_r)$ is $\sigma_v(I_rK_r)\phi_e^{\omega i\sigma}=\sigma\phi_e^{-\omega i\sigma}$. Definition of σ is drawn for $\omega=0$ states from the spectroscopic notation $(\pm)$ of the state. However, for $\omega\neq0$, it is necessary to fix (arbitrarily) the relative sign of $\phi_e^{-\omega i\sigma}$ with respect to $\phi_e^{\omega i\sigma}$ to obtain the value of σ.

For a given total angular momentum quantum number J and projection M over the SF frame $\mathbf{K_L}$ axis, a natural basis to expand the total wavefunction is given by[33]

$$|JM;\Omega\omega ji\sigma\rangle\propto D^{J*}_{M\Omega}(\varphi_R,\theta_R,\varphi_r)D^{j*}_{\Omega\omega}(0,\theta_r,0)\phi_e^{\omega i\sigma}, \tag{A3}$$

where D symbols stand for Wigner rotation matrices.[34] Note that here and below, we use the symbol ''$\propto$'' instead of ''$=$'' to avoid explicit normalization constants. The functions $|JM;\Omega\omega ji\sigma\rangle$ are not eigenfunctions of parity $\mathbf{\Pi}$ and identical particles permutation $\mathbf{P}$ operators. Transformations of the functions (A3) under the action of these operators is shown in the Table III.

It is, however, possible to build from these functions the new ones which are eigenfunctions of these operators, with eigenvalues ϵ_Π, $\epsilon_P=\pm1$.

2. Parity

Parity operator $\mathbf{\Pi}$ changes all electronic and nuclear coordinates in SF frame to their opposite. This operator does not modify the SF frame, so $(\theta_R,\varphi_R)\rightarrow(\pi-\theta_R,\pi+\varphi_R)$. From Eq. (A1), one sees that the BF frame is transformed as $(\mathbf{I_R},\mathbf{J_R},\mathbf{K_R})\rightarrow(\mathbf{I_R},-\mathbf{J_R},-\mathbf{K_R})$. The $\mathbf{r}$ vector is changed to its opposite, which, in the BF frame, corresponds to a change of sign of its X coordinate with two others being unchanged. As a result, $(\theta_r,\varphi_r)\rightarrow(\theta_r,\pi-\varphi_r)$. According to Eq. (A2), the MF frame is changed as $(\mathbf{I_r},\mathbf{J_r},\mathbf{K_r})\rightarrow(-\mathbf{I_r},\mathbf{J_r},-\mathbf{K_r})$. Thus, parity changes an electronic vector to its opposite in the SF frame, but its net effect in the MF frame is the change of sign of its Y coordinate with two others being unchanged. The effect of parity on the electronic wave function in the MF frame is thus equivalent to $\sigma_v(\mathbf{I_r},\mathbf{K_r})$.

The eigenfunctions of the parity operators are built as

$$(1+\epsilon_\Pi \mathbf{\Pi})|JM;\Omega\omega ji\sigma\rangle$$
$$\propto D^{J*}_{M\Omega}(\varphi_R,\theta_R,\varphi_r)D^{j*}_{\Omega\omega}(0,\theta_r,0)\phi_e^{\omega i\sigma}+\epsilon_\Pi\sigma(-1)^{J-\omega}$$
$$\times D^{J*}_{M-\Omega}(\varphi_R,\theta_R,\varphi_r)D^{j*}_{-\Omega-\omega}(0,\theta_r,0)\phi_e^{-\omega i\sigma}, \quad \text{(A4)}$$

where the relation $D^{j*}_{\Omega\omega}(0,\theta_r,0)=(-1)^{\Omega-\omega}D^{j*}_{-\Omega-\omega}(0,\theta_r,0)$ has been used. Both states $|JM;\Omega\omega i\sigma\rangle$ and $|JM;-\Omega-\omega i\sigma\rangle$ produce the same parity adapted state through Eq. (A4). We can therefore restrict ourselves to $\Omega\geqslant 0$ in the following.

An alternative way of writing the symmetry adapted basis functions of Eq. (A4), with the advantage of simplifying the evaluation of some matrix elements of the Hamiltonian, especially the potential ones, can be obtained as follows. First, parity adapted electronic wave functions $\phi_e^{\bar{\omega}i\bar{\sigma}}(\bar{\omega}=|\omega|,\bar{\sigma}=\pm 1)$ are defined as

$$\phi_e^{\bar{\omega}i\bar{\sigma}}=\frac{1}{[2(1+\delta_{\omega 0})]^{1/2}}(\phi_e^{\omega i\sigma}+\sigma\bar{\sigma}\phi_e^{-\omega i\sigma}). \quad \text{(A5)}$$

We use this definition for $\omega\geqslant 0$. Indeed, using Eq. (A5) with $\omega<0$ would produce the same set of states, but with different signs. We have $\sigma_v(\mathbf{I_r},\mathbf{K_r})\phi_e^{\bar{\omega}i\bar{\sigma}}=\bar{\sigma}\phi_e^{\bar{\omega}i\bar{\sigma}}$, which justifies that these electronic functions are the eigenfunctions of the single geometric operation which leaves the three-body coplanar system invariant, namely, symmetry through the molecular plane. We also introduce parity adapted Wigner functions ($\bar{\Omega}=|\Omega|$, $\epsilon=\pm 1$):

$$D^{J\epsilon*}_{M\bar{\Omega}}(\varphi_R,\theta_R,\varphi_r)=\frac{1}{[2(1+\delta_{\Omega 0})]^{1/2}}[D^{J*}_{M\Omega}(\varphi_R,\theta_R,\varphi_r)$$
$$+\epsilon D^{J*}_{M-\Omega}(\varphi_R,\theta_R,\varphi_r)] \quad \text{(A6)}$$

for $\Omega\geqslant 0$ case. Equation (A4) can be rewritten in terms of these new functions. We have to distinguish two cases when ω is positive or negative. Writing $\omega=\epsilon_s\bar{\omega}$, $\epsilon_s=\text{sign}(\omega)$, we obtain from Eq. (A4) the parity adapted electronic-angular basis functions as

$$|JM\epsilon_\Pi;\bar{\Omega}\bar{\omega}\epsilon_s ji\rangle$$
$$\propto D^{J\epsilon_R*}_{M\bar{\Omega}}(\varphi_R,\theta_R,\varphi_r)D^{j*}_{\bar{\Omega}\epsilon_s\bar{\omega}}(0,\theta_r,0)\phi_e^{\bar{\omega}i\bar{\sigma}}$$
$$+\epsilon_s D^{J-\epsilon_R*}_{M\bar{\Omega}}(\varphi_R,\theta_R,\varphi_r)D^{j*}_{\bar{\Omega}\epsilon_s\bar{\omega}}(0,\theta_r,0)\phi_e^{\bar{\omega}i-\bar{\sigma}}, \quad \text{(A7)}$$

where

$$\epsilon_R=\epsilon_\Pi\bar{\sigma}(-1)^{J+\bar{\Omega}}. \quad \text{(A8)}$$

3. Permutation

Permutation **P** of the two identical atoms *B* modifies neither the **R** vector nor the BF frame, so that $(\theta_R,\varphi_R)\rightarrow(\theta_R,\varphi_R)$. It changes **r** to its opposite, so that $(\theta_r,\varphi_r)\rightarrow(\pi-\theta_r,\pi+\varphi_r)$. From Eq. (A2), one sees that the MF frame is changed as $(\mathbf{I}_r,\mathbf{J}_r,\mathbf{K}_r)\rightarrow(\mathbf{I}_r,-\mathbf{J}_r,-\mathbf{K}_r)$. An electronic vector, unchanged in the SF frame through the permutation operation, has its *Y* and *Z* components changed to their opposite in the MF frame so that **P** is equivalent to a rotation over π around the $\mathbf{I}_r$ vector which we denote $C_2(\mathbf{I}_r)$.

Eigenfunctions of permutation operator are built as $(1+\epsilon_P\mathbf{P})|JM\epsilon_\Pi;\bar{\Omega}\bar{\omega}\epsilon_s ji\rangle$. The action of **P** on the electronic wave function is obtained using $C_2(\mathbf{I}_r)=iC_2(\mathbf{K}_r)\sigma_v(\mathbf{I}_r,\mathbf{K}_r)$ so that $C_2(\mathbf{I}_r)\phi_e^{\bar{\omega}i\bar{\sigma}}=i\bar{\sigma}(-1)^{\bar{\omega}}\phi_e^{\bar{\omega}i\bar{\sigma}}$. Therefore,

$$\mathbf{P}|JM\epsilon_\Pi;\bar{\Omega}\bar{\omega}\epsilon_s ji\rangle$$
$$=i\bar{\sigma}(-1)^{\bar{\omega}}(-1)^j|JM\epsilon_\Pi;\bar{\Omega}\bar{\omega}-\epsilon_s ji\rangle$$

and we can keep only $\epsilon_s=1$ to generate the permutation adapted basis functions. Application of $(1+\epsilon_P\mathbf{P})$ yields

$$|JM\epsilon_\Pi\epsilon_P;\bar{\Omega}\bar{\omega}ji\rangle$$
$$\propto D^{J\epsilon_R*}_{M\bar{\Omega}}(\varphi_R,\theta_R,\varphi_r)D^{j\epsilon_r*}_{\bar{\Omega}\bar{\omega}}(0,\theta_r,0)\phi_e^{\bar{\omega}i\bar{\sigma}}$$
$$+D^{J-\epsilon_R*}_{M\bar{\Omega}}(\varphi_R,\theta_R,\varphi_r)D^{j\epsilon_r*}_{\bar{\Omega}\bar{\omega}}(0,\theta_r,0)\phi_e^{\bar{\omega}i-\bar{\sigma}}, \quad \text{(A9)}$$

where

$$\epsilon_r=\epsilon_P\bar{\sigma}i(-1)^{j+\bar{\omega}}. \quad \text{(A10)}$$

This final expression has been used in FWP and BSWP calculations. Notice that the functions $D^{j\epsilon_r*}_{\bar{\Omega}\bar{\omega}}(0,\theta_r,0)$ are symmetric or antisymmetric with respect to the operation $\theta_r\rightarrow\pi-\theta_r$. From $D^{j*}_{\bar{\Omega}\bar{\omega}}(0,\pi-\theta_r,0)=(-1)^{j+\bar{\Omega}}D^{j*}_{\bar{\Omega}-\bar{\omega}}(0,\theta_r,0)$ one sees that the symmetry of $D^{j*}_{\bar{\Omega}\bar{\omega}}$ with respect to this operation is $\epsilon_r(-1)^{j+\bar{\Omega}}=\epsilon_P\bar{\sigma}i(-1)^{\bar{\Omega}}(-1)^{\bar{\omega}}$.

For $\bar{\Omega}=0$ or $\bar{\omega}=0$, only one of the two terms in the sum in Eq. (A9) survives. When $\bar{\Omega}=0$, this is the term for which $\epsilon_R=+1$, i.e., $\bar{\sigma}=\epsilon_\Pi(-1)^J$ [see Eq. (A8)]. When $\bar{\omega}=0$, the $\bar{\sigma}$ component which survives is defined by the electronic wave function ($\pm$ state). In both cases, $D^{j\epsilon_r*}_{\bar{\Omega}=0\bar{\omega}}(0,\theta_r,0)$ is nonzero only when $\epsilon_r=(-1)^{\bar{\omega}}$. From Eq. (A10), this gives $(-1)^j=\epsilon_P\bar{\sigma}i$. In other words, the choice of permutation symmetry ϵ_P determines a choice on the parity of the rotational quantum number *j* in these cases.

4. Hamiltonian matrix elements

The electronic Hamiltonian H_{el} couples only states with identical *J*, $M\epsilon_\Pi$, ϵ_P, $\bar{\Omega}$, and $\bar{\sigma}$. These nonvanishing electronic matrix elements are given by

$$\langle JM\epsilon_\Pi\epsilon_P;\bar{\Omega}\bar{\omega}ji|H_{\text{el}}|JM\epsilon_\Pi\epsilon_P;\bar{\Omega}\bar{\omega}'j'i'\rangle$$
$$\propto\langle D^{j\epsilon_r*}_{\bar{\Omega}\bar{\omega}}(0,\theta_r,0)|H_{\text{el}}^{\bar{\sigma};\bar{\omega}i,\bar{\omega}'i'}|D^{j\epsilon_r*}_{\bar{\Omega}\bar{\omega}'}(0,\theta_r,0)\rangle$$
$$+\langle D^{j-\epsilon_r*}_{\bar{\Omega}\bar{\omega}}(0,\theta_r,0)|H_{\text{el}}^{-\bar{\sigma};\bar{\omega}i,\bar{\omega}'i'}|D^{j-\epsilon_r*}_{\bar{\Omega}\bar{\omega}'}(0,\theta_r,0)\rangle. \quad \text{(A11)}$$

When $\bar{\Omega}=0$ or $\bar{\omega}=0$, only one of the two terms in Eq. (A11) does not vanish. Each term involves an integral over θ_r. This integral is nonzero if the integrand is symmetric with respect to $\theta_r\rightarrow\pi-\theta_r$ transformation. If we denote $s^{\bar{\sigma};\bar{\omega}i,\bar{\omega}'i'}$ the symmetry of $H_{\text{el}}^{\bar{\sigma};\bar{\omega}i,\bar{\omega}'i'}$ with respect to this operation, knowing that the symmetry of $D^{j\epsilon_r*}_{\bar{\Omega}\bar{\omega}}$ is $\epsilon_P\bar{\sigma}i(-1)^{\bar{\Omega}}(-1)^{\bar{\omega}}$, we obtain $s^{\bar{\sigma};\bar{\omega}i,\bar{\omega}'i'}=ii'(-1)^{\bar{\omega}}(-1)^{\bar{\omega}'}$ as a necessary condition for H_{el} to couple the states

with the same permutation symmetry. As an example of this relation for the ArI_2 case, we see that the $B(0_u^+)/B''(1_u)$, $B(0_u^+)/1(2_g)$, and $B(0_u^+)/a'(0_g^+)$ couplings are all antisymmetric with respect to $\theta_r=\pi/2$ transformation. On the other hand, the $B(0_u^+)/a(1_g)$ coupling is symmetric (the same results, of course, follows from the symmetry analysis of the DIM PT1 diabatic couplings[7,15]).

The angular momentum operators matrix elements are given by

$$\langle JM\epsilon_\Pi\epsilon_P;\overline{\Omega}\overline{\omega}ji|\mathbf{N}^2|JM\epsilon_\Pi\epsilon_P;\overline{\Omega}\overline{\omega}ji\rangle\propto j(j+1)-\overline{\omega}^2 \tag{A12}$$

and

$$\begin{aligned}\langle JM\epsilon_\Pi\epsilon_P;\overline{\Omega}\overline{\omega}ji|\mathbf{l}^2|JM\epsilon_\Pi\epsilon_P;\overline{\Omega}'\overline{\omega}ji\rangle&\propto\delta_{\overline{\Omega}',\overline{\Omega}}[J(J+1)\\&+j(j+1)-2\overline{\Omega}^2]\\&\propto\delta_{\overline{\Omega}',\overline{\Omega}\pm1}\sqrt{J(J+1)-\overline{\Omega\Omega}'}\sqrt{j(j+1)-\overline{\Omega\Omega}'},\end{aligned} \tag{A13}$$

where the $\mathbf{j}_e$ Coriolis couplings between different electronic states have been neglected and the diagonal matrix elements have been approximated by $\langle\mathbf{j}_e\rangle\approx\overline{\omega}^2$.

[1] A. A. Buchachenko, N. Halberstadt, B. Lepetit, and O. Roncero, Int. Rev. Phys. Chem. **22**, 153 (2003).
[2] M. L. Burke and W. Klemperer, J. Chem. Phys. **98**, 6642 (1993).
[3] D. M. Willberg, M. Gutmann, J. J. Breen, and A. H. Zewail, J. Chem. Phys. **96**, 198 (1992).
[4] O. Roncero, N. Halberstadt, and J. A. Beswick, in *Reaction Dynamics in Clusters and Condensed Phases*, edited by J. Jortner, R. D. Levine, and B. Pullmann (Kluwer, Dordrecht, 1994), p. 73.
[5] O. Roncero, N. Halberstadt, and J. A. Beswick, Chem. Phys. Lett. **226**, 82 (1994).
[6] O. Roncero, N. Halberstadt, and J. A. Beswick, J. Chem. Phys. **104**, 7554 (1996).
[7] A. A. Buchachenko, Chem. Phys. Lett. **292**, 273 (1998).
[8] A. Bastida, J. Zúñiga, A. Requena, N. Halberstadt, and J. A. Beswick, Chem. Phys. **240**, 229 (1999).
[9] S. K. Gray, Chem. Phys. Lett. **197**, 86 (1992).
[10] S. K. Gray and O. Roncero, J. Phys. Chem. **99**, 2512 (1995).
[11] O. Roncero and S. K. Gray, J. Chem. Phys. **104**, 4999 (1996).
[12] E. M. Goldfield and S. K. Gray, J. Chem. Soc., Faraday Trans. **93**, 909 (1997).
[13] E. M. Goldfield and S. K. Gray, Chem. Phys. Lett. **276**, 1 (1997).
[14] O. Roncero, B. Lepetit, J. A. Beswick, N. Halberstadt, and A. A. Buchachenko, J. Chem. Phys. **115**, 6961 (2001).
[15] B. Lepetit, O. Roncero, A. A. Buchachenko, and N. Halberstadt, J. Chem. Phys. **116**, 8367 (2002).
[16] L. Veseth, J. Phys. B **6**, 1473 (1973).
[17] A. A. Buchachenko and N. F. Stepanov, J. Chem. Phys. **104**, 9913 (1996).
[18] A. A. Buchachenko, O. Roncero, and N. F. Stepanov, Russ. J. Phys. Chem. **74**, S193 (2000).
[19] E. A. Pazyuk, A. V. Stolyarov, V. I. Pupyshev, N. F. Stepanov, S. Ya. Umanskii, and A. A. Buchachenko, Mol. Phys. **99**, 91 (2001).
[20] H. Tal-Ezer and R. Kosloff, J. Chem. Phys. **81**, 3967 (1984).
[21] P. Pernot and J. A. Lester, Int. J. Quantum Chem. **40**, 577 (1991).
[22] G. G. Balint-Kurti, R. N. Dixon, and C. C. Marston, J. Chem. Soc., Faraday Trans. **86**, 1741 (1990).
[23] P. Villarreal, S. Miret-Artés, O. Roncero, G. Delgado-Barrio, J. A. Beswick, N. Halberstadt, and R. D. Coalson, J. Chem. Phys. **94**, 4230 (1991).
[24] S. B. Woodruff and D. L. Thompson, J. Chem. Phys. **71**, 376 (1979).
[25] L. D. Landau, Phys. Z. Sowjetunion **2**, 46 (1932).
[26] C. Zener, Proc. R. Soc. London, Ser. A **137**, 696 (1932).
[27] G. Kubiak, P. Fitch, L. Wharton, and D. H. Levy, J. Chem. Phys. **68**, 4477 (1978); D. H. Levy, Adv. Chem. Phys. **47**, 323 (1981).
[28] O. Roncero, P. Villarreal, G. Delgado-Barrio, N. Halberstadt, and K. C. Janda, J. Chem. Phys. **99**, 1035 (1993); O. Roncero, D. Caloto, K. C. Janda, and N. Halberstadt, *ibid.* **107**, 1406 (1997).
[29] K. E. Johnson, W. Sharfin, and D. H. Levy, J. Chem. Phys. **74**, 163 (1981).
[30] A. E. Stevens Miller, C. Chuang, H. Fu, K. F. Higgins, and W. Klemperer, J. Chem. Phys. **111**, 7844 (1999).
[31] J. A. Blazy, B. M. DeKoven, T. D. Russel, and D. H. Levy, J. Chem. Phys. **72**, 2439 (1980).
[32] A. Burroughs and M. C. Heaven, J. Chem. Phys. **114**, 7027 (2001).
[33] M. L. Dubernet, D. Flower, and J. M. Hutson, J. Chem. Phys. **94**, 7602 (1991).
[34] R. N. Zare, *Angular Momentum* (Wiley, New York, 1988).
[35] S. K. Gray, S. A. Rice, and M. J. Davis, J. Phys. Chem. **90**, 3470 (1986); S. K. Gray and S. A. Rice, Faraday Discuss. Chem. Soc. **82**, 307 (1986); S. K. Gray, J. Chem. Phys. **87**, 2051 (1987); S. H. Tersigni and S. A. Rice, Ber. Bunsenges. Phys. Chem. **92**, 227 (1986); C. E. Wozny and S. K. Gray, *ibid.* **92**, 236 (1986); S. H. Tersigni, P. Gaspard, and S. A. Rice, J. Chem. Phys. **92**, 1775 (1990); M. Zhao and S. A. Rice, *ibid.* **96**, 198 (1992); A. A. Buchachenko and N. F. Stepanov, *ibid.* **98**, 5486 (1993); A. A. Granovsky, A. V. Medvedev, A. A. Buchachenko, and N. F. Stepanov, *ibid.* **108**, 6282 (1998).